Solution Conformation of [AF]dG Opposite a −1 Deletion Site in a DNA Duplex: Intercalation of the Covalently Attached Aminofluorene Ring into the Helix with Base Displacement of the C^8-Modified *Syn* Guanine into the Major Groove†

Bing Mao,‡ Monique Cosman,‡ Brian E. Hingerty,§ Suse Broyde,|| and Dinshaw J. Patel*,‡

Cellular Biochemistry and Biophysics Program, Memorial Sloan-Kettering Cancer Center, New York, New York 10021, Health Sciences Research Division, Oak Ridge National Laboratory, Oak Ridge, Tennessee 37831, and Biology Department, New York University, New York, New York 10003

Received January 4, 1995; Revised Manuscript Received March 2, 1995⊗

ABSTRACT: This paper reports on the solution structure of the [AF]dG adduct positioned opposite a deletion site in a DNA oligomer duplex that defines the alignment of the covalent aminofluorene−C^8-guanine adduct relative to the deletion site. The combined NMR molecular mechanics computational studies were undertaken on the [AF]dG adduct embedded in the d(C5-[AF]G6-C7)·d(G16-G17) sequence context in a duplex containing 11 residues on the modified strand and 10 on the partner, with no base opposite the modification. The exchangeable and nonexchangeable protons of the aminofluorene moiety and the nucleic acid were assigned following analysis of two-dimensional NMR data sets in H_2O and D_2O solution. The solution conformation of the [AF]dG·del 11-mer duplex has been determined by incorporating intramolecular and intermolecular proton−proton distances defined by lower and upper bounds deduced from NOESY spectra as restraints in molecular mechanics computations in torsion angle space. The aminofluorene ring of [AF]dG6 is intercalated between intact Watson−Crick dC5·dG17 and dC7·dG16 base pairs with the guanine base of [AF]dG6 in a *syn* alignment displaced into the major groove. The *syn* glycosidic torsion angle at [AF]dG6 is supported by both carbon and proton chemical shift data for the sugar resonances of the modified guanine residue. The long axis of the aminofluorene ring is parallel to the long axis of the flanking dG·dC base pairs with the AF ring undergoing rapid 180° flips on the NMR time scale. The intercalation site is wedge shaped with a pronounced propeller-twisting and buckling of the dC5·dG17 base pair. The guanine base of [AF]dG6, which is positioned in the major groove, is inclined relative to the helix axis and stacks over the 5′-flanking dC5 residue in the solution structure. The intercalative-base displacement structure of the [AF]dG·del 11-mer duplex exhibits several unusually shifted proton resonances that can be readily accounted for by the ring current contributions of the guanine purine and carcinogen fluorene aromatic rings of the [AF]dG6 adduct. There are similarities between this structure of the AF-C^8-dG covalent adduct positioned opposite a deletion site and the (+)-*trans-anti*-BP-N^2-dG covalent adduct positioned opposite a deletion site in the same sequence context reported previously from this laboratory [Cosman et al. (1994) *Biochemistry 33*, 11507−11517]. The chromophores are intercalated into the helix opposite the deletion site with displacement of the modified guanine into the major groove in both cases. The important difference is that the modified guanine of the N^2-linked benzo[*a*]pyrenyl-dG adduct adopts an *anti* alignment while it adopts a *syn* alignment for the C^8-linked aminofluorene adduct, both of which have their guanine bases tilted relative to the helix axis and stacked over the major groove edge of the 5′-flanking dC5 residue.

2-Aminofluorene (AF) and 2-acetylaminofluorene (AAF) are members of a class of chemical carcinogens, the aromatic amines, that are widely present in the environment as products of fossil fuel combustion, tobacco smoke, dyes, and barbecued meat and fish. AF and AAF are synthetic prototypes that were developed more than 50 years ago as insecticides. Their use for this purpose was quickly discontinued once it was determined that their chemically activated derivatives are carcinogenic. Instead, these substances have become models for the investigation of the biochemical mechanisms of cancer induction by aromatic amines. The extensive literature on AF and AAF has recently been reviewed (Heflich & Neft, 1994).

Activated forms of AF and AAF react with DNA, yielding major adducts to the C^8-position of guanine that have been identified both *in vitro* and *in vivo*. Mutational consequences of these adducts have been determined *in vitro* and *in vivo* in bacterial and mammalian systems (Bichara & Fuchs, 1985; Moriya et al., 1988; Carothers et al., 1989; Burnouf et al., 1989; Gupta et al., 1989, 1991; Belguise-Valladier et al., 1991, 1994; Mah et al., 1991; Lambert et al., 1992; Shibutani & Grollman, 1993; Garcia et al., 1993; Melchior et al., 1994; Tebbs et al., 1994; Napolitano et al., 1994; Thomas et al., 1994). The mutagenesis data is complex and varies from system to system. Each adduct is capable of inducing

† This research is supported by NIH Grant CA-49982 to D.J.P., by NIH Grant CA-28038, NIH Grant RR-06458, and DOE Grant DE-FG02-90ER60931 to S.B., and by DOE Contract DE-AC05-840R21400 with Martin-Marietta Energy Systems and DOE OHER Field Work Proposal ERKP931 to B.E.H.

‡ Memorial Sloan-Kettering Cancer Center.
§ Oak Ridge National Laboratory.
|| New York University.

⊗ Abstract published in *Advance ACS Abstracts,* May 1, 1995.

0006-2960/95/0434-6226$09.00/0

frameshift and point mutations depending on context, although AAF has a greater tendency to induce frameshifts, while AF has a greater tendency to induce point mutations.

The focus of the present work is on [AF]dG adducts positioned opposite −1 deletion sites. These are especially intriguing because a slipped mutagenic replication intermediate (Streisinger et al., 1966), in which the modified guanine is bulged out, has been proposed as an explanation for −1 deletions in specific contexts (Kunkel, 1990; Schaaper et al., 1990; Lambert et al., 1992; Shibutani & Grollman, 1993; Napolitano et al., 1994). Consequently, solution structures of such duplexes are of great interest. We have in previous work elucidated structures for the (+)-*trans-anti-* and (+)-*cis-anti-*[BP]dG•del adducts derived from the covalent binding of (+)-*anti*-benzo[*a*]pyrene diol epoxide (BPDE) to the N^2-position of guanine positioned opposite −1 deletion sites (Cosman et al., 1994a,b), using the same DNA sequence context as in the current contribution. Deletion of the residue normally present opposite the BPDE-modified guanine resulted in a greater thermodynamic stabilization of the modified duplex relative to the unmodified control duplex (Ya et al., 1994).

Solution structural studies for AF modified duplexes have previously been reported in the context of a mismatch in which an adenine was positioned opposite the modified guanine (Norman et al., 1989) or with the normal cytosine partner (Cho et al., 1994; Eckel & Krugh, 1994). The present work provides a solution structural characterization of [AF]-dG adduct **1** positioned opposite a deletion site in the sequence context d(C5-[AF]G6-C7)•d(G16-G17) **2** at the DNA oligonucleotide duplex level.

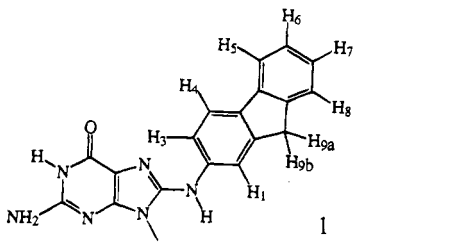

1

C1 – C2 – A3 – T4 – C5 – * G6 – C7 – T8 – A9 – C10 – C11

G21 – G20 – T19 – A18 – G17 —— G16 – A15 – T14 – G13 – G12

2

MATERIALS AND METHODS

Oligonucleotide Synthesis. The deoxyoligonucleotides d(C-C-A-T-C-G-C-T-A-C-C) and d(G-G-T-A-G-G-A-T-G-G) were synthesized on an Applied Biosystems Model 392 DNA synthesizer and purified by reverse-phase HPLC.

Preparation of Adduct. The d(C-C-A-T-C-G-C-T-A-C-C) sequence was converted into the d(C-C-A-T-C-[AF]G-C-T-A-C-C) adduct sequence as described previously (Norman et al. 1989). Briefly, in the first step the oligonucleotide was reacted with 8 molar equiv of N-acetoxy-AAF in 2 mM sodium citrate (pH 7.0) containing 30% ethanol at 37 °C for 3 h to produce the [AAF]dG modified oligomer. The purified [AAF]dG modified oligomer (using reverse-phase HPLC) was then converted to [AF]dG modified oligomer by dissolving in 1 M NaOH containing 0.3% 2-mercaptoethanol at a concentration of 2 mg/mL for 45 min at room temperature. The [AF]dG modified oligomers were further purified by reverse-phase HPLC, desalted on Sephadex G-25, and converted to sodium form on Dowex 50×8 cation exchange resin.

The d(C-C-A-T-C-[AF]G-C-T-A-C-C) 11-mer strand was annealed with the complementary d(G-G-T-A-G-G-A-T-G-G) 10-mer strand at 70 °C, and the stoichiometry was followed by monitoring single proton resonances in both strands.

Sample Preparation. The NMR spectra of the [AF]dG•del 11-mer duplex (3 mM in duplex) and the corresponding control dG•del 11-mer duplex (3 mM in duplex) were recorded in 0.1 M NaCl, 10 mM phosphate, and 1 mM EDTA solution containing either D_2O or 90:10 H_2O/D_2O (v/v). All NMR spectra were recorded on samples at pH 7.0.

Optical Melting Experiments. The optical melting transitions on the control dG•del 11-mer and [AF]dG•del 11-mer duplexes at 10 μM concentration (in strands) were undertaken in 100 mM NaCl and 20 mM phosphate, pH 7.0. The order−disorder transition was monitored at 260 nm with a heating rate of 1 °C/min.

NMR Experiments. All NMR data sets were recorded on Varian Unity Plus 600 and 500 MHz NMR spectrometers. A combination of through-space nuclear Overhauser effect (NOESY) and through-bond correlated (COSY, TOCSY) two-dimensional spectra were recorded and analyzed to assign the aminofluorene and nucleic acid protons in the [AF]-dG•del 11-mer duplex.

Proton NOESY spectra in H_2O buffer were collected with 150 ms mixing time at 1 °C. The carrier frequency was placed directly on the HOD signal, and an optimized jump-return pulse sequence was used for solvent suppression. The proton NOESY spectra in D_2O were collected with mixing times of 50, 90, 140, 170, 200, and 300 ms. The carrier frequency was set on the residual HOD resonance, which was presaturated during a 2.0 s relaxation delay between scans. The through-bond TOCSY spectra were recorded in D_2O buffer at spin lock times of 40 and 80 ms.

The indirect detected proton−phosphorus correlation spectrum was recorded on the [AF]dG•del 11-mer duplex in D_2O at 25 °C using the pulse sequence described by Sklenar et al. (1986). Both proton and phosphorus sweep widths were set to 6 ppm with a 1.3 s presaturation of the HOD residual resonance. The phosphorus spectra were referenced relative to external 10% trimethylphosphate (TMP).

Proton−carbon HMQC correlation spectra on the [AF]-dG•del 11-mer duplex were recorded in D_2O buffer at 25 °C. The proton carrier frequency was set to 4.5 ppm with a sweep width of 8.5 ppm while the ^{13}C carrier frequency was set to 67.0 ppm with a sweep width of 66.0 ppm. The carbon spectra were referenced relative to external 3-(trimethylsilyl)propionate (TSP) using the method described by Bax and Subramanian (1986).

The volume integrals of NOE cross-peaks as a function of five mixing times (50, 90, 140, 170, and 200 ms) were measured to generate the build-up curves for nonexchangeable protons in D_2O solution. The interproton distances were calculated based on the two spin approximation using dT-(NH3)-dA(H2) fixed distance of 2.92 Å for NOESY data sets in H_2O and dC(H5)-dC(H6) fixed distance of 2.45 Å for NOESY data sets in D_2O solution. The upper and lower bound ranges on the estimated interproton distances for nonexchangeable protons were determined based on the

resolution of the cross-peaks in the two-dimensional contour plots and the quality of the NOE build-up plots.

The base proton to sugar H1′ proton NOE cross-peaks in the shortest mixing time NOESY data set in D_2O were evaluated to qualitatively differentiate between *syn* (strong NOE) and *anti* (weak NOE) glycosidic torsion angles (Patel et al., 1982). The proton−proton vicinal coupling constants among sugar protons were analyzed from phase-sensitive COSY spectra to qualitatively distinguish between the C3′-*endo* and C2′-*endo* family of sugar puckers. The relative intensity of the NOE cross-peaks between base protons and their own and 5′-flanking sugar H2′, H2″, and H3′ protons were also used to qualitatively distinguish between the A- and B-DNA family of helices for the modified duplex (van der Ven & Hilbers, 1988).

Molecular Mechanics Computations. Minimized potential energy calculations were carried out with DUPLEX, a molecular mechanics program for nucleic acids that performs potential energy minimizations in the reduced variable domain of torsion angle space (Hingerty et al., 1989). The advantage of torsion space, compared to Cartesian space minimizations, is the vast diminution in the number of variables that must be simultaneously optimized, thereby permitting larger movements from a given starting conformation during minimization as well as the assurance of correct internal geometry and chirality.

DUPLEX uses a potential set similar to the one developed by Olson and co-workers for nucleic acids (Taylor & Olson, 1983) for which details have been published previously (Hingerty et al., 1989). Geometry and force field parameters, including partial charges, for the [AF]dG adduct were the same as those employed previously (Hingerty & Broyde, 1982; Broyde & Hingerty, 1983). A hydrogen-bond penalty function (Hingerty et al., 1989) was employed in all first stage minimizations to aid the minimizer in locating the Watson−Crick hydrogen-bonded structures indicated by the NMR data. To locate minimum energy conformations with interproton distances available from the experimental NMR data, pseudo-potentials (permitting upper and lower bound restraints) were added to the energy as described previously (Norman et al., 1989; Schlick et al., 1990; Cosman et al., 1993). Briefly, the following functions were used:

$$F_N = W_N \sum_1^n (d - d_N)^2 \quad (1)$$

$$F_{NN} = W_{NN} \sum_1^n (d - d_{NN})^2 \quad (2)$$

The *W*s are adjustable weights (in the range of 10−30 kcal/mol·Å^2). Weights in this range serve to guide the minimizer toward the structure defined by the NMR data, while permitting the force field, whose predictive capabilities have been demonstrated (Hingerty et al., 1989; Singh et al., 1991) to play its part. d is the current value of the interproton distance, d_N is a target upper bound, and d_{NN} is a target lower bound. Equation 1 is implemented when d is greater than d_N, and eq 2 is implemented when d is less than d_{NN}. The functions are summed over all n target distances. All penalty functions were released in the last minimization steps to yield unrestrained final structures that are minimum energy conformations. F_N and F_{NN} can also be employed as relative indices of goodness-of-fit to the NMR data. Here the d values are the achieved distances in a given model, and the *W*s are the weights employed in the search. F_N and F_{NN} are composites, reflecting the overall fit of all the achieved distances to their targets. They both adopt values of zero when all model distances are within the upper and lower NMR distance bounds. Small deviations from the NMR targets, within the uncertainty of the data, are accepted in computed models, and these therefore have non-zero F_N and F_{NN} values. Computations were carried out at the Department of Energy's National Energy Research Supercomputer Center and the National Science Foundation's San Diego Supercomputer Center.

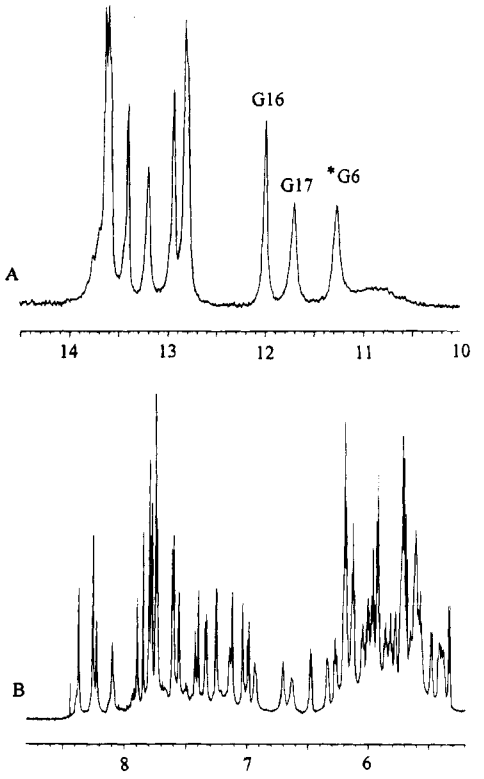

FIGURE 1: (A) Imino proton spectra (10.0−14.5 ppm) of the [AF]-dG·del 11-mer duplex in H_2O buffer at 1 °C and (B) nonexchangeable proton spectra (5.2−8.8 ppm) of the [AF]dG·del 11-mer duplex in D_2O buffer at 25 °C. The buffer was 0.1 M NaCl, 10 mM phosphate, and 0.1 mM EDTA, at pH 7.0. The imino proton assignments of the [AF]dG6, dG16, and dG17 are shown over the resonances in the spectrum.

RESULTS

We have measured the thermal transition midpoints (t_m) at optical concentrations (~10 μM in strands) for the control dG·del 11-mer duplex (t_m = 24 °C) and the [AF]dG·del 11-mer duplex (t_m = 37.5 °C). The observed stabilization on adduct formation permits us to undertake NMR studies (at 3 mM concentrations) on the [AF]dG·del 11-mer duplex at ambient temperature.

Exchangeable Nucleic Acid Protons. The exchangeable proton NMR spectrum (10.0−14.5 ppm) of the [AF]dG·del 11-mer duplex in H_2O buffer, pH 7.0, at 1 °C is plotted in Figure 1A. Eleven partially resolved exchangeable protons are detected between 10.0 and 14.5 ppm including three well-resolved upfield-shifted imino protons at 11.26, 11.69, and 11.98 ppm. The imino protons have been assigned following an analysis of the 150 ms mixing time NOESY spectrum of

the adduct duplex in H_2O buffer solution at 1 °C. We detect imino to imino NOE connectivities between adjacent base pairs along the length of the modified duplex except between the dG16, [AF]dG6, and dG17 residues centered about the lesion site. These NOE cross-peaks are traced in the expanded NOESY contour plot of the symmetrical 11.0−14.0 ppm region in Figure 2C with no NOE detected between the two upfield-shifted imino protons of dG17 (11.69 ppm) and dG16 (11.98 ppm) (boxed region, Figure 2C).

The expanded NOESY contour plot (150 ms mixing time) establishing the NOE connectivities between the imino protons (11.0−14.0 ppm) and amino protons (4.7−8.7 ppm) in the [AF]dG•del 11-mer duplex is plotted in Figure 2B. The four thymine protons (13.39, 13.56, 13.58, and 13.62 ppm) exhibit NOEs to the adenine H2 protons within individual dA•dT pairs (peaks G−J, respectively, Figure 2B). The guanine imino protons exhibit NOEs to the hydrogen-bonded and exposed cytosine amino protons within individual dG•dC base pairs (peaks A/A′, B/B′, C/C′, D/D′, E/E′, and F/F′ in Figure 2B). These results establish Watson−Crick base pairing at all six dG•dC pairs and all four dA•dT base pairs in the [AF]dG•del 11-mer duplex.

The remaining guanine imino proton at 11.26 ppm is assigned to [AF]dG6 positioned opposite the deletion site in the adduct duplex. It exhibits an NOE to its own averaged amino protons at 6.31 ppm (peak K, Figure 2B) and also a strong NOE to the H_2O resonance (peak L, Figure 2B). Its upfield shift and rapid exchange with H_2O suggest that this guanine imino proton of [AF]dG6 positioned opposite the deletion site most likely loops out of the helix and is accessible to solvent in the [AF]dG•del 11-mer duplex.

The imino protons of [AF]dG6 at the lesion site as well as those of terminal residues dG12 and dG21 broaden significantly on raising the temperature of the [AF]dG•del 11-mer duplex from 1 to 15 °C (supplementary Figure S1). This reflects the lability of these imino protons to exchange with solvent water. We also note that the 11.69 ppm imino proton of dG17 is broader than the 11.98 ppm imino proton of dG16 in the 1 °C spectrum (Figure 1A). This relative pattern of line widths persists in the 15 °C spectrum (Figure S1).

The exchangeable proton chemical shifts for the central d(C5-[AF]G6-C7)•d(G16-G17) segment of the [AF]dG•del 11-mer duplex are listed in Table 1 and for the entire adduct duplex in supplementary Table S1. The chemical shift changes for the central segment on proceeding from the control duplex (dG6 opposite deletion site) to the adduct duplex ([AF]dG6 opposite deletion site) are listed in supplementary Table S2.

The observed NOE patterns establish the formation of intact Watson−Crick dC7•dG16 and dC5•dG17 base pairs on either side of the [AF]dG6 lesion positioned opposite the −1 deletion site. The observed upfield shifts of the guanine imino and hydrogen-bonded cytosine amino protons for the dC7•dG16 and dC5•dG17 base pairs (Table S2) suggest that the aminofluorene ring is most likely intercalated between these base pairs, which flank the [AF]dG6 lesion site.

Exchangeable Aminofluorene Protons. The single NH proton on the aminofluorene ring, which is linked to the C^8 position within [AF]dG6, is assigned a chemical shift of 7.64 ppm following an analysis of the cross-peaks between the aminofluorene H1 and H3 protons and the NH proton in the NOESY spectrum of the adduct duplex in H_2O buffer

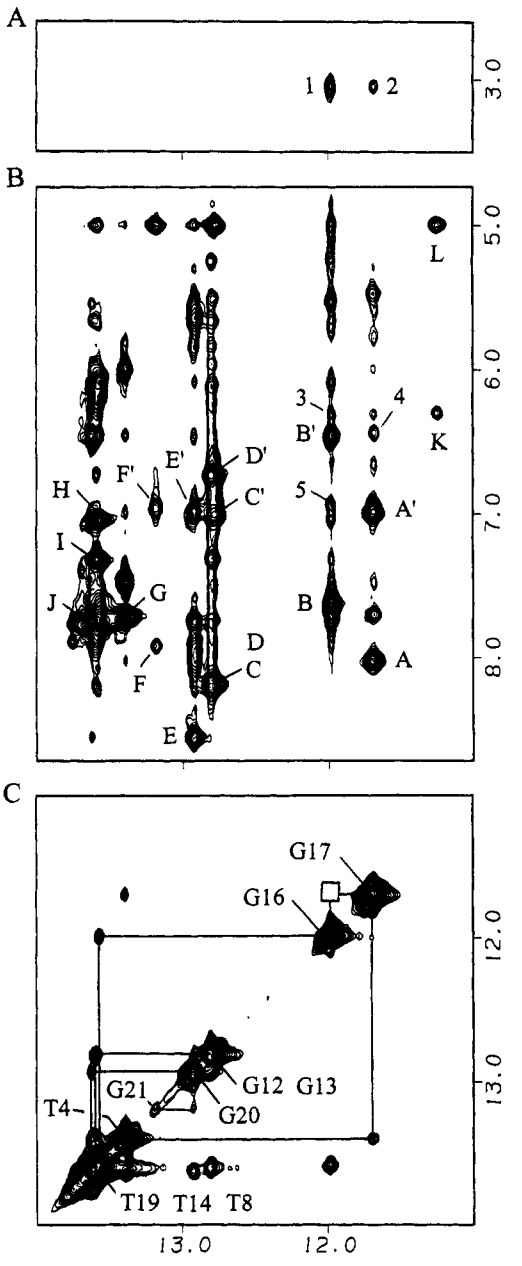

FIGURE 2: Expanded NOESY (150 ms mixing time) contour plots of the [AF]dG•del 11-mer duplex in H_2O buffer at 1 °C. (A) NOE connectivities between the imino protons (11.0−14.0 ppm) and the AF methylene protons (2.5−3.5 ppm). The carcinogen-DNA cross-peaks 1 and 2 are assigned as follows: 1, G16(NH1)-AF(H9a,b); 2, G17(NH1)-AF(H9a,b). (B) NOE connectivities between the imino protons (11.0−14.0 ppm) and the base and amino protons regions (4.7−8.7 ppm). The NOE cross-peaks involving the imino protons are labeled in the figure as follows: A,A′, G17(NH1)-C5-(NH_2-4b,e); B,B′, G16(NH1)-C7(NH_2-4b,e); C,C′, G12(NH1)-C11-(NH_2-4b,e); D,D′, G13(NH1)-C10(NH_2-4b,e); E,E′, G20(NH1)-C2(NH_2-4b,e); F,F′, G21(NH1)-C1(NH_2-4b,e); G, T4(NH3)-A18(H2); H, T8(NH3)-A15(H2); I, T14(NH3)-A9(H2); J, T19(NH3)-A3(H2); K, [AF]G6(NH1)-[AF]G6(NH_2-2); L, [AF]G6(NH1)-H_2O. The carcinogen-DNA NOE cross-peaks 3−5 are assigned as follows: 3, G16(NH1)-AF(H8); 4, G17(NH1)-AF(H5); 5, G16-(NH1)-AF(H3,H4). (C) NOE connectivities in the symmetrical (10.0−14.0 ppm) region. The imino assignments are labeled along the diagonal. The lines trace the NOE connectivities between adjacent base pairs starting at dG21 toward one end of the helix and proceeding to dG13 toward the other end of the helix. The connectivity between the imino protons of dG16 and that of dG17 is missing and marked by a box.

Table 1: Proton Chemical Shifts of the d(C5-[AF]G6-C7)·d(G16-G17) Segment of the [AF]dG·del 11-mer Duplex in Aqueous Buffer

Exchangeable Proton Chemical Shifts (ppm) at 1 °C			
	G(NH1)	G(NH_2-2)	C(NH_2-4)
dC5·dG17	11.69		6.97,[a] 8.01[b]
[AF]dG6·del	11.26	6.31	
dC7·dG16	11.98		6.47,[a] 7.62[b]

Nonexchangeable Proton Chemical Shifts (ppm) at 25 °C						
	H8/H6	H2/H5	H1′	H2′,H2″	H3′	H4′
dC5	6.63	5.47	5.81	1.40, 2.11	4.51	3.94
[AF]dG6			6.12	3.34, 2.72	5.00	4.69
dC7	7.73	5.58	5.77	2.47, 2.26	4.51	4.27
dG16	7.39		5.61	2.36, 2.31	4.99	4.26
dG17	7.89		5.37	2.69, 2.75	4.96	4.33

[a] Exposed amino proton. [b] Hydrogen-bonded amino proton.

solution at 1 °C. The assignment of the H1 and H3 protons of aminofluorene can be rigorously established from an analysis of the NOESY and COSY spectra of the [AF]dG·del 11-mer duplex recorded in D_2O buffer (see below).

Nonexchangeable Nucleic Acid Protons. The nonexchangeable proton spectrum (5.2−8.8 ppm) of the [AF]-dG·del 11-mer duplex in D_2O, pH 7.0, at 25 °C is plotted in Figure 1B. The well-resolved nucleic acid base and sugar protons as well as the aminofluorene protons were assigned based on an analysis of through-space distance connectivities in NOESY data sets as a function of mixing time and through-bond connectivities in COSY and TOCSY data sets recorded in D_2O buffer, pH 7.0, at 25 °C.

The expanded NOESY (300 ms mixing time) contour plot establishing sequential connectivities between the base protons (6.3−8.4 ppm) and the sugar H1′ and cytosine H5 protons (5.2−6.8 ppm) of the [AF]dG·del 11-mer duplex in D_2O buffer, pH 7.0, at 25 °C is plotted in Figure 3. The NOE connectivities from the base proton (purine H8 or pyrimidine H6) to its own and 5′-flanking sugar H1′ protons have been traced along the duplex from dC1 to dC11 on the modified strand and from dG12 to dG21 on the complementary strand. This tracing is shown for the central segment extending from dA3 to dT8 on the modified strand (solid line, Figure 3) and from dA15 to dA18 on the unmodified complementary strand (dashed line, Figure 3). The interruption in the tracing at the dC5-[AF]dG6 step on the modified strand is due to the absence of a purine H8 proton following AF modification at the C^8-position of dG6 in the adduct duplex. A weak connectivity is observed at the dG16-dG17 step on the unmodified complementary strand (see arrow, Figure 3). These base and sugar H1′ proton assignments have been confirmed by cross checks in other regions of the NOESY contour plot as well as from COSY and TOCSY plots to yield a complete set of base and sugar H1′, H2′, H2″, H3′, and H4′ proton assignments for the [AF]-dG·del 11-mer duplex.

The nonexchangeable proton chemical shifts for the central d(C5-[AF]G6-C7)·d(G16-G17) segment in the [AF]dG·del 11-mer duplex are listed in Table 1. The nonexchangeable base and sugar proton chemical shift assignments for the entire adduct duplex are listed in supplementary Table S3. Proton chemical shift differences for the central segment between the adduct duplex and the unmodified control duplex are given in supplementary Table S2.

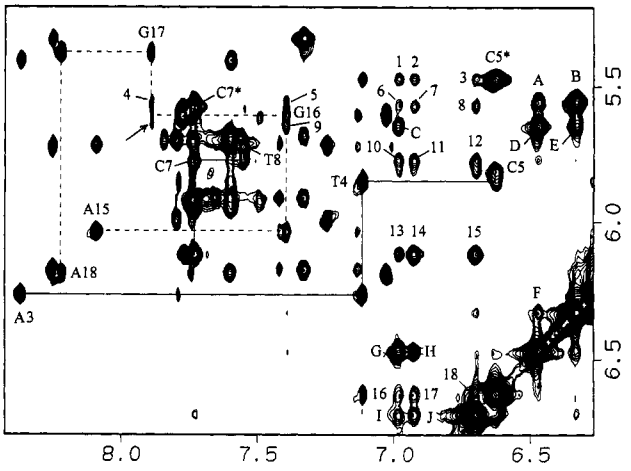

FIGURE 3: Expanded NOESY (300 ms mixing time) contour plot of the [AF]dG·del 11-mer duplex in D_2O buffer at 25 °C establishing distance connectivities between the base (purine H8 and pyrimidine H6) protons (6.3−8.4 ppm) and the sugar H1′ and deoxycytidine H5 protons (4.5−6.8 ppm). The NOE connectivities between the base and their own and the 5′-flanking sugar H1′ protons from dA3 to dT8 on the modified strand are shown by solid lines and from dA15 to dA18 on the unmodified partner strand are shown by dashed lines. The assignments label the base to their own sugar H1′NOEs, while the deoxycytidine H6-H5 NOEs are designated by asterisks. Note the unusual upfield shift of the H6 proton of dC5 to 6.63 ppm. Note that the NOE cross-peak at the dC5-[AF]-dG6 is missing because of the absence of an H8 proton for [AF]-dG6 while the NOE corresponding to the dG16-dG17 step is weak (labeled by arrow). The carcinogen-carcinogen NOE cross-peaks A−G between aminofluorene protons are assigned as follows: A, AF(H7)-AF(H5); B, AF(H7)-AF(H8); C, AF(H6)-AF(H4); D, AF-(H6)-AF(H5); E, AF(H6)-AF(H8); F, AF(H8)-AF(H5); G, AF(H5)-AF(H4); H, AF(H5)-AF(H3); I, AF(H1)-AF(H4); J, AF(H1)-AF(H3). The carcinogen-DNA NOE cross-peaks 1−18 are assigned as follows: 1, C5(H5)-AF(H4); 2, C5(H5)-AF(H3); 3, C5(H5)-AF(H1); 4, AF(H7)-G17(H8); 5, AF(H7)-G16(H8); 6, C7(H5)-AF-(H4); 7, C7(H5)-AF(H3); 8, C7(H5)-AF(H1); 9, AF(H6)-G16(H8); 10, C7(H1′)-AF(H4); 11, C7(H1′)-AF(H3); 12, C7(H1′)-AF(H1); 13, [AF]G6(H1′)-AF(H4); 14, [AF]G6(H1′)-AF(H3); 15, [AF]G6-(H1′)-AF(H1); 16, C5(H6)-AF(H4); 17, C5(H6)-AF(H3); 18, C5-(H6)-AF(H1). The chemical shift values for the aminofluorene protons are as follows: AF(H1), 6.71 ppm; AF(H3), 6.93 ppm; AF(H4), 6.99 ppm; AF(H5), 6.47 ppm; AF(H6), 5.65 ppm; AF-(H7), 5.56 ppm; AF(H8), 6.33 ppm; AF(H9a,b), 3.07 ppm; AF-(NH), 7.64 ppm.

We observe a strong NOE between the H5 proton of dC7 and the H1′ proton of [AF]dG6 (peak A, supplementary Figure S2) and also between the H6 proton of dC7 and the H4′ proton of [AF]dG6 (peak B, Figure S2) for the [AF]-dG6-dC7 step in both 50 and 300 ms mixing time NOESY spectra of the adduct duplex in D_2O solution. These results suggest that the major groove edge (contains H6 and H5 base protons) of the dC7 base is close to the minor groove face (contains H1′ and H4′ sugar protons) of the [AF]dG6 sugar ring in the [AF]dG·del 11-mer duplex.

It should be noted that relative to the control duplex, large upfield chemical shift differences are observed on adduct formation at the H6 (−0.74 ppm) base as well as the H2′ (−0.57 ppm) and H3′ (−0.24 ppm) sugar protons of the dC5 residue (Table S2) located 5′ to the lesion site on the modified strand. By contrast, downfield shifts are observed on adduct formation at the H2′ (+0.79 ppm), H4′ (+0.36 ppm), and H1′ (+0.19 ppm) sugar protons of the [AF]dG6 residue (Table S2). Further, we observe an inversion in the characteristic H2′ and H2″ sugar cross-peak patterns at the lesion site with the H2′ proton chemical shift (3.34 ppm) of

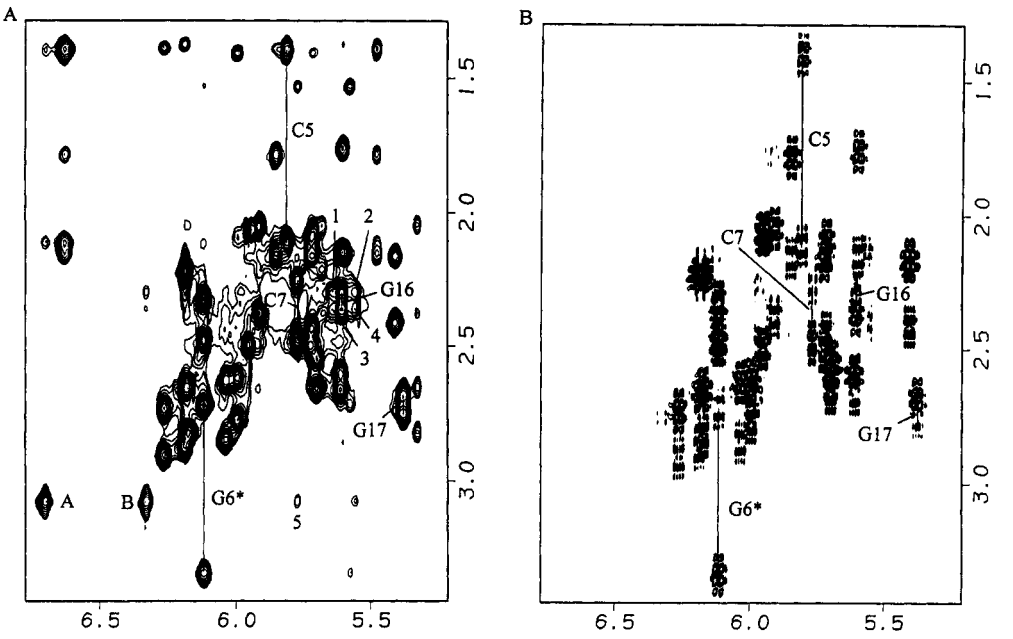

FIGURE 4: (A) Expanded NOESY (300 ms mixing time) contour plots of the [AF]dG•del 11-mer duplex in D_2O buffer at 25 °C showing NOE between the sugar H1′ protons (5.2−6.8 ppm) and H2′,H2″ protons (1.3−3.5 ppm). The NOE cross-peaks A and B between aminofluorene protons are assigned as follows: A, AF(H1)-AF(H9a,b); B, AF(H8)-AF(H9a,b). The carcinogen-DNA NOE cross-peaks 1−5 are assigned as follows: 1, G16(H2″)-AF(H6); 2, G16(H2″)-AF(H7); 3, G16(H2′)-AF(H6); 4, G16(H2′)-AF(H7); 5, AF(H9a,b)-C7-(H1′). (B) Expanded phase-sensitive COSY contour plot of the [AF]dG•del 11-mer duplex in D_2O buffer at 25 °C, establishing coupling connectivities between the H1′ protons (5.2−6.8 ppm) and H2′,H2″ protons (1.3−3.5 ppm).

[AF]dG6 shifting dramatically downfield in the adduct duplex (Figure 4).

Nonexchangeable Aminofluorene Protons. The nonexchangeable aminofluorene protons were assigned from an analysis of through-bond and through-space two-dimensional spectra on the [AF]dG•del 11-mer duplex recorded in D_2O buffer, pH 7.0, at 25 °C. The H1, H3, and H4 protons are differentiated from H5−H8 protons by coupling patterns observed in COSY and TOCSY spectra and from NOE cross-peaks observed in NOESY spectra. The H1 and H8 protons were assigned based on NOEs to the H9a,b protons within the aminofluorene ring. The aminofluorene proton chemical shifts in the [AF]dG•del 11-mer duplex are listed in the caption to Figure 3. The temperature dependence of the line widths of aminofluorene ring protons in the [AF]dG•del 11-mer duplex in D_2O buffer can be monitored in spectra recorded at 1, 15, and 35 °C (supplementary Figure S3).

Carbon Spectra. An expanded contour plot of a natural abundance proton−carbon HMQC correlation experiment on the [AF]dG•del 11-mer duplex in D_2O buffer, pH 7.0, at 25 °C is plotted in Figure 5A. This expanded contour plot correlates the H1′ and C1′ chemical shifts of individual residues for the adduct duplex. The cross-peaks for the d(T4-C5-[AF]G6-C7-T8)•d(A15-G16-G17-A18) segment are assigned and labeled in Figure 5A. We note that the C1′ chemical shift of [AF]dG6 (88.88 ppm) is ~5 ppm downfield of its neighboring dG16 (84.16 ppm) and dG17 (84.23 ppm) residues in the adduct duplex (Figure 5A). A downfield shift of ~5 ppm in the ^{13}C chemical shift at the C1′ sugar position could either originate in an *anti* to *syn* glycosidic torsion angle change without a change in sugar pucker (Ghose et al., 1994; Greene et al., 1995) or alternately reflect a C2′-*endo* to C3′-*endo* sugar pucker change without a change in the glycosidic torsion angle (Varani & Tinoco, 1991). The vicinal proton coupling constant data places the [AF]dG6 sugar pucker in the C2′-*endo* range, and hence the ~5 ppm downfield shift points toward a *syn* glycosidic torsion angle for [AF]dG6 in the [AF]dG•del 11-mer duplex in solution.

Phosphorus Spectra. The proton decoupled phosphorus spectrum of the [AF]dG•del 11-mer duplex has been recorded in D_2O buffer, pH 7.0, at 25 °C. The phosphorus resonances are dispersed over a 1 ppm range with several resonances shifted to low and high field of the −4.0 to −4.5 ppm spectral region characteristic of an unperturbed phosphorus B-DNA backbone. The phosphorus resonances have been assigned following an analysis of the proton detected phosphorus−proton heteronuclear correlation experiment with the expanded contour plot shown in Figure 5B. Each phosphorus resonance exhibits cross-peaks to the 5′-linked H3′ proton and the 3′-linked H4′ and H5′,5″ protons. The phosphorus resonances are assigned on the basis of the known H3′ and H4′ proton assignments in the adduct duplex. The phosphorus assignments for the central five base pair fragment of the adduct duplex are listed in Figure 5B. The phosphorus chemical shifts for the dC5-[AF]dG6 and dG16-dG17 steps are shifted to low field while that for the dC7-dT8 step is shifted to high field of the unperturbed phosphorus chemical shift range. We observe down field shifts at dC5-[AF]dG6 (~0.6 ppm) and dG16-dG17 (~0.6 ppm) steps while an upfield shift is observed at the dC7-dT8 step (~0.4 ppm) on proceeding from the control duplex to the adduct duplex.

Carcinogen-DNA NOEs and Restraints. We observe a set of carcinogen-DNA NOEs between aminofluorene and nucleic acid protons in the [AF]dG•del 11-mer duplex that have been categorized based on whether they involve exchangeable or nonexchangeable protons. Several of these carcinogen-DNA NOEs are labeled with numbers in the expanded NOESY contour plots in Figures 2−4, and their assignments are listed in the figure captions. The corresponding carcinogen-DNA intermolecular distance restraints deduced from NOE build-up curves for nonexchangeable

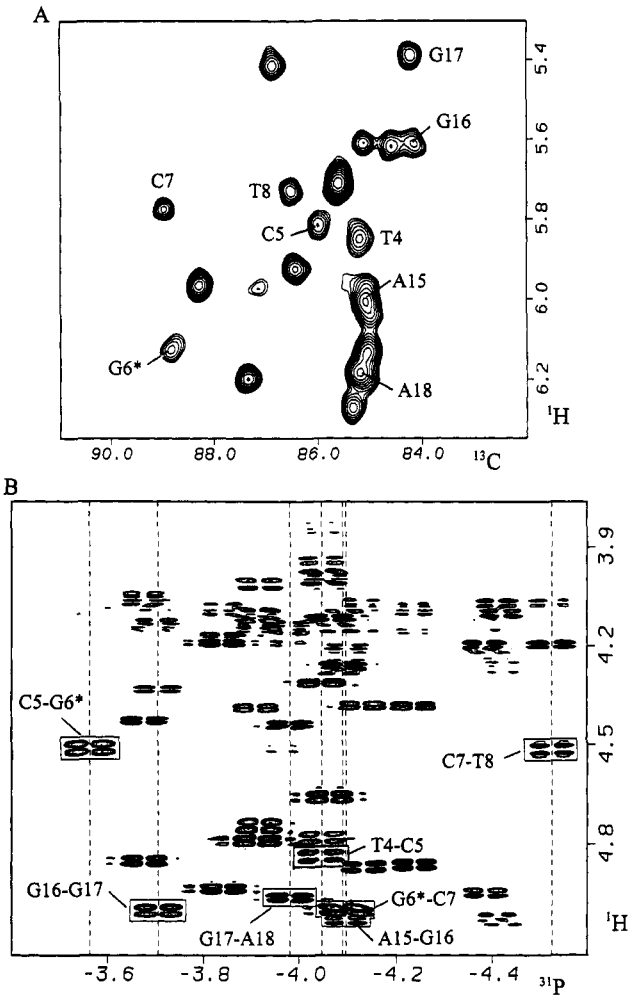

FIGURE 5: (A) Expanded contour plot of ^{1}H−^{13}C heteronuclear multiple-quantum coherence (HMQC) experiment on the [AF]-dG-del 11-mer duplex in D_2O buffer at 25 °C. The C1′ assignments are marked for the d(T4-C5-[AF]G6-C7-T8)·d(A15-G16-G17-A18) segment. (B) Expanded contour plot of the proton-detected phosphorus−proton heteronuclear correlation experiment on the [AF]dG-del 11-mer duplex in D_2O buffer at 25 °C. The phosphorus assignments are listed for steps centered about the lesion site. The correlation cross-peaks between the phosphorus and its 5′-flanking sugar H3′ protons are boxed.

protons and defined by lower and upper bounds in the [AF]-dG-del 11-mer duplex are listed in Table 2.

We observe NOEs between the aminofluorene H6 and H7 protons at the [AF]dG6 lesion site and the sugar (H2′, H2″, and H3′) protons of dG16 as well as to the H8 base protons of dG16 and dG17 in the adduct duplex. These NOEs establish that the aminofluorene ring edge furthest from the covalent linkage site is positioned near the base and sugar protons of the dG16-dG17 step on the partner strand of the [AF]dG-del 11-mer duplex. Further, the observed NOEs between the aminofluorene H3/H4, H5, H8, and H9a,b protons and the imino protons of dG16 and dG17 place the aminofluorene between the dC5·dG17 and dC7·dG16 base pairs in the adduct duplex. The long axis of the aminofluorene ring must be approximately parallel to the long axis of the flanking base pairs, if its H6 and H7 protons are to interact with the partner strand across from the lesion site.

The observed large upfield chemical shift of the H6 proton (−0.74 ppm) located on the major groove edge of dC5 combined with moderate upfield shifts for all remaining dC5 sugar protons requires that the modified guanine be displaced into the major groove and positioned over the major groove base edge and sugar ring of dC5 in the adduct duplex. This alignment can only be achieved if the [AF]dG6 adopts a *syn* glycosidic torsion angle in the adduct duplex.

The observed pattern of carcinogen-DNA NOEs between the protons on different edges of aminofluorene ring and the central d(C5-[AF]G6-C7)·d(G16-G17) segment define two alignments of the intercalated aminofluorene ring opposite the deletion site in the adduct duplex. In one alignment, the AF(H1) proton exhibits NOEs to the minor groove sugar protons of dC5 (H1′ and H2″ protons), [AF]dG6 (H1′ proton), and dC7(H1′ proton), while the AF(H3) and AF-(H4) protons exhibit NOEs to the major groove edge protons of dC5 and dC7 (H5 proton) in the adduct duplex (Table 2). These NOE patterns indicate that the aminofluorene ring is intercalated between the dC5·dG17 and dC7·dG16 base pairs with the C^9-containing edge directed toward the minor groove in the adduct duplex. In the second alignment, we also observe that the AF(H3) proton exhibits NOEs to the minor groove sugar protons of dC5 (H1′ and H2″ protons), [AF]-dG6 (H1′ proton), and dC7(H1′ proton), while the AF(H1) proton exhibits NOEs to the major groove edge protons of dC5 and dC7 (H5 protons) in the adduct duplex (Table 2). These NOE patterns indicate that the C^9-containing edge is directed toward the major groove. Further, these two sets of NOE patterns are also present for adduct duplex NOESY spectra recorded at lower mixing times excluding contributions from spin diffusion effects. These observations establish the existence of two conformations in fast exchange on the NMR time scale that are related by 180° flips along the long axis of the intercalated aminofluorene ring in the adduct duplex.

Of the 32 carcinogen-DNA restraints for the adduct duplex listed in Table 2, excluding restraints labeled with "a", 27 are assigned to the conformer (designated structure **1**) where the C^9-containing edge of the aminofluorene is directed toward the major groove. The same number of restraints for the adduct duplex, excluding restraints labeled with "b" in Table 2, is assigned to the conformer (designated structure **2**) where the C^9-containing edge of the aminofluorene is directed toward the minor groove.

Molecular Mechanics Computations. The search strategy employed began with a B-DNA (Arnott et al., 1976) central three base pair d(C5-[AF]G6-C7)·d(G16-G17) segment of the [AF]dG-del 11-mer duplex. The computations were guided by the restraints listed in Table 2 that had been assigned to this conformer (bounds labeled by "a" in Table 2 were not used in the calculation). The AF-DNA orientation space was searched with 16 energy minimization trials in which the linkage torsion angles α′-([AF]dG6(N^9)-[AF]dG6-(C^8)-[AF](N)-[AF](C^2)) and β′-([AF]dG6(C^8)-[AF](N)-[AF]-(C^2)-[AF](C^1)) were each started at 0, 90, 180, and 270° in all combinations, and the DNA starting conformation was the B-form except for a *syn* ($\chi = 60$) glycosidic torsion for the [AF]dG6 residue as required by the experimental ^{13}C chemical shift data. Searching orientation space at 90° intervals of α′ and β′ is a robust procedure for locating all the important potential energy wells because our minimization protocol permits torsion angle variations of up to 100° in each minimization step (Hingerty et al., 1989). Consequently, energy minima in each quadrant of α′ and β′ are accessible, and the reduced variable domain of torsion angle

Table 2: Comparison of Input Carcinogen-DNA Distance Bounds with Those Observed for the Unrestrained Solution Structure of the [AF]dG·del 11-mer Duplex

	carcinogen-DNA distances (Å)		
	exptl bounds	observed	
		structure **1**	structure **2**
exchangeable protons (carcinogen-DNA)			
[AF]G6(H1′)-AF(NH)	2.0−4.0	2.89	2.90
G16(NH1)-AF(H3,H4)	2.5−5.5	4.44, 3.47	5.76, 5.17
G16(NH1)-AF(H8)	3.5−5.5	6.36	4.49
G16(NH1)-AF(H9a,b)	2.5−4.5	5.97, 4.98	2.44, 3.99
G17(NH1)-AF(H5)	3.5−5.5	3.92	5.01
G17(NH1)-AF(H9a,b)	4.0−5.5	5.14, 6.23	5.37, 3.97
nonexchangeable protons (DNA-DNA)			
[AF]G6(H1′)-C7(H5)	2.0−3.2	2.77	2.92
[AF]G6(H1′)-C7(H6)	2.5−3.5	3.27	3.61
[AF]G6(H4′)-C7(H6)	2.5−4.0	3.54	3.73
G16(H1′)-G17(H8)	>5.5	6.73	6.30
nonexchangeable protons (carcinogen-DNA)			
C5(H5)-AF(H1)	3.5−5.0	3.13	3.66
C5(H5)-AF(H3)	3.5−5.0	3.83	3.14
C5(H5)-AF(H4)	3.5−5.0	4.56	3.88
C5(H2′)-AF(H1)	3.2−5.0[a]	6.96	*5.49*
C5(H2″)-AF(H1)	3.0−5.0[a]	7.03	*4.78*
[AF]G6(H1′)-AF(H1)	2.5−3.7[a]	5.15	*2.26*
[AF]G6(H1′)-AF(H3)	2.5−3.5[b]	*2.32*	5.08
[AF]G6(H1′)-AF(H4)	3.0−5.5[b]	*4.67*	6.65
C7(H1′)-AF(H1)	3.0−5.5[a]	8.82	*5.54*
C7(H1′)-AF(H3)	3.0−5.5[b]	*5.37*	9.22
C7(H1′)-AF(H4)	3.0−5.5[b]	*5.54*	9.48
C7(H5)-AF(H1)	3.0−5.0	5.23	*3.76*
C7(H5)-AF(H3)	3.0−5.0	*3.72*	5.66
G16(H8)-AF(H6)	3.2−4.2[a]	4.87	*3.79*
G16(H8)-AF(H7)	3.2−4.5[b]	*3.42*	5.27
G16(H2′)-AF(H6)	2.5−4.0	2.51	2.26
G16(H2′)-AF(H7)	2.5−4.0	2.31	2.75
G16(H2″)-AF(H6)	2.5−4.0	3.41	3.57
G16(H2″)-AF(H7)	2.5−4.0	3.90	2.92
G16(H3′)-AF(H6)	3.5−5.0	4.64	4.06
G16(H3′)-AF(H7)	3.5−5.0	3.44	4.92
G17(H8)-AF(H7)	4.0−5.5	3.70	3.55

[a] Bounds that are not used in structure **1** calculations. [b] Bounds that are not used in structure **2** calculations.

space greatly enhances the likelihood of finding the important structures. In these trials, the DUPLEX hydrogen-bond penalty function (Hingerty et al., 1989) for Watson−Crick base pairing was utilized at the dC5·dG17 and dC7·dG16 base pairs, since the NMR data indicated that these hydrogen bonds were present. The calculations were guided by NMR-derived upper and lower bound distance restraints listed in Table 2.

Of the 16 computed structures of the d(C5-[AF]G6-C7)·d(G16-G17) segment, one structure had the lowest energy and best combined goodness-of-fit indices. This structure had an energy of −71.1 kcal/mol and goodness-of-fit values for eqs 1 and 2 of 9.0 and 2.3, respectively, with $W = 15$ kcal/mol·Å^2. The second best structure had an energy of −58.5 kcal/mol and goodness-of-fit indices for eqs 1 and 2 of 8.8 and 3.6, respectively. Two superpositioned views of the d(C5-[AF]G6-C7)·d(G16-G17) segment for these two structures (RMSD = 0.623Å) are plotted in Figure 6. The lowest energy structure was then subjected to one further refinement: the original list of NMR restraints had not been able to distinguish the AF(H9a) and AF(H9b) protons, and restraints were given for G16(NH1) and G17(NH1) to both of these protons. In the lowest energy structure, AF(H9a)-G16(NH1) and AF(H9b)-G17(NH1) fell within the data bounds while AF(H9b)-G16(NH1) and AF(H9a)-G17(NH1) did not. Consequently, the latter restraints were removed in an additional minimization, producing a structure with energy of −79.8 kcal/mol and goodness-of-fit indices for eqs 1 and 2 of 2.1 and 1.6, respectively. This d(C5-[AF]G6-C7)·d(G16-G17) segment was employed in building the [AF]dG·del 11-mer duplex. For this purpose, an unmodified energy-minimized B-form dG·del 11-mer duplex was first computed. The d(C5-[AF]G6-C7)·d(G16-G17) segment was then embedded in the dG6·del 11-mer duplex by replacement of residues dC5, dG6, and dC7 and their partners dG16 and dG17, followed by energy minimization with restraints. Subsequently, the hydrogen-bond penalty function and the distance restraints were released with energy minimization in one step, yielding a final unrestrained minimum energy structure of the [AF]dG·del 11-mer duplex in which the C^9-containing edge of aminofluorene faces the major groove (designated Structure 1).

The NMR data had indicated the presence of a second conformer with the C^9-containing edge of aminofluorene facing the minor groove, resulting from an approximately 180° flip of the AF ring about its long axis. A starting structure was created with this orientation from the d(C5-[AF]G6-C7)·d(G16-G17) segment of Structure 1 by rotating the torsion angle β'-([AF]dG(C^8)-[AF](N)-[AF](C^2)-[AF](C^1)) by 180°. This structure was then minimized with the restraints listed in Table 2 that had been assigned to this second conformer (bounds labeled by "b" in Table 2 were

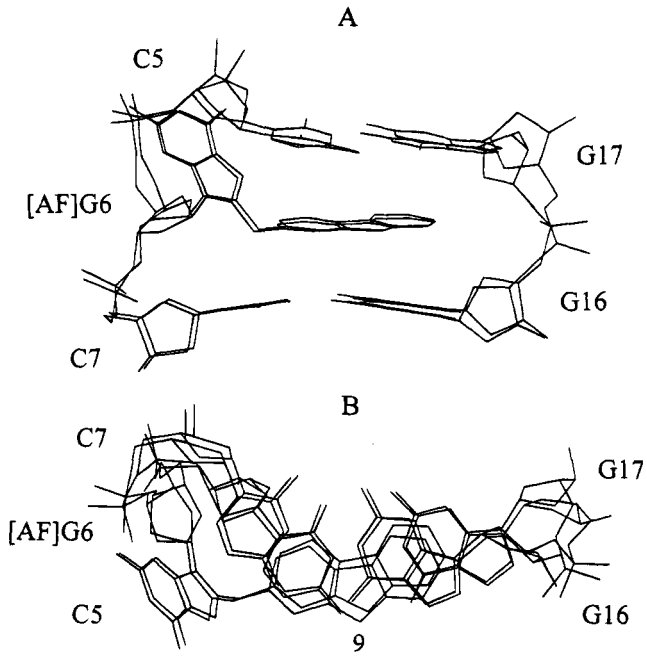

FIGURE 6: Superposition of the two d(C5-[AF]G6-C7)•d(G16-G17) trinucleotide segments that best fit the NMR data of the [AF]dG•del 11-mer duplex obtained from the 16 trials to search conformational space using NMR restraints (Table 2) and program DUPLEX. (A) View looking into the major groove and normal to the helix axis of the central trinucleotide segments and (B) view looking down the helix axis of the same segments.

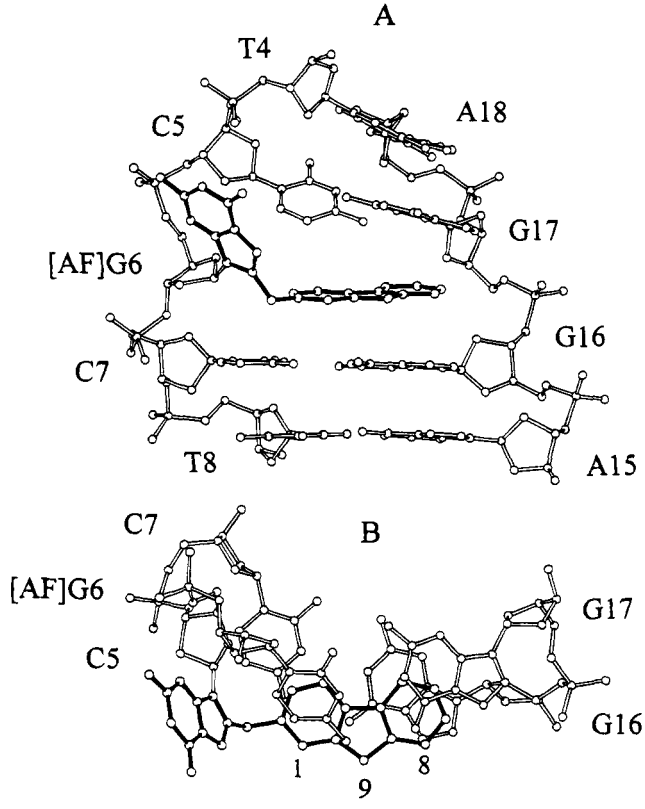

FIGURE 7: (A) Views looking into the major groove and normal to the helix axis of the central d(T4-C5-[AF]G6-C7-T8)•d(A15-G16-G17-A18) segment of structure **1** with the C^9-containing edge of AF directed toward the major groove in the [AF]dG•del 11-mer duplex. The AF ring system is shown in darkened bonds and is intercalated between the dC5•dG17 and dC7•dG16 base pairs. The modified dG6 base is displaced into the major groove and is directed toward its 5′-neighbor dC5 in the sequence. (B) Views looking down the helix axis for the d(C5-[AF]G6-C7)•d(G16-G17) segment in the structure **1** of the [AF]dG•del 11-mer duplex. Figures were prepared using Molscript VI.1 (Kraulis, 1991).

not used in the calculation). The resulting d(C5-[AF]G6-C7)•d(G16-G17) segment had an energy of −82 kcal/mol with goodness-of-fit indices for eqs 1 and 2 of 2.0 and 1.5, respectively, with $W = 15$ kcal/mol•Å^2. This structure was then built into the dG•del 11-mer duplex level with the same procedure that was employed for structure **1**, described above, yielding a final unrestrained minimum energy structure of the [AF]dG•del 11-mer duplex in which the C^9-containing edge of aminofluorene faces the minor groove (designated structure **2**).

Solution Structures of the [AF]dG•del Adduct Duplex. Views normal to the helix axis and looking into the major groove of the central d(T4-C5-[AF]G6-C7-T8)•d(A15-G16-G17-A18) segment of the lowest energy NMR/energy-minimized structures of the [AF]dG•del 11-mer duplex are shown for structure **1** in Figure 7A and for structure **2** in Figure 8A. The corresponding structures for the entire duplexes are shown in supplementary Figures S4 and S5, respectively. In both structures, the covalently linked aminofluorene ring intercalates between flanking Watson–Crick dC5•dG17 and dC7•dG16 base pairs by displacing the guanine ring of [AF]dG6 into the major groove (Figures 7A and 8A). The major groove face of the sugar ring of dC5 is positioned over the guanine base plane of [AF]dG6, which is directed toward the 5′-end of the modified strand and tilted relative to the helix axis for both structures (Figures 7A and 8A). The dC5•dG17 pair is propeller-twisted by −29.5° and buckled by 29.4° for structure **1** (Figure 7A) while it is propeller-twisted by −38.7° and buckled by 36.3° for structure **2** (Figure 8A) [computed using the approach of Babcock et al. (1993)].

Views looking down the helix axis of the central d(C5-[AF]G6-C7)•d(G16-G17) segment of the NMR/energy-minimized structures of the [AF]dG•del 11-mer duplex are shown for structure **1** in Figure 7B and for structure **2** in Figure 8B. These views emphasize the overlap geometry between the aminofluorene ring system and the flanking dC5•dG17 and dC7•dG16 base pairs. The long axis of the aminofluorene ring of AF is approximately parallel to the long axis of the dC5•dG17 and dC7•dG16 base pairs for both structures (Figures 7B and 8B).

The carcinogen-base linkage site for the [AF]dG6 residues is defined by the torsion angles α′-([AF]dG6(N^9)-[AF]dG6-(C^8)-[AF](N)-[AF](C^2)) and β′-([AF]dG6(C^8)-[AF](N)-[AF]-(C^2)-[AF](C^1)). These α′ and β′ angles adopt values of 90° and 109° in structure **1** and of 92° and 283° in structure **2**. The $\beta' = 109°$ orientation directs the C^9-containing edge of aminofluorene toward the major groove (Figure 7B), while the $\beta' = 283°$ value has this edge directed toward the minor groove (Figure 8B) for the [AF]dG•del 11-mer duplex. Thus, the pair of conformers are related by an ~180° rotation about the AF long axis that is reflected in the β′ values. The glycosidic torsion angles, sugar puckers, and backbone torsion angles for the d(T4-C5-[AF]G6-C7-T8)•d(A15-G16-G17-A18) segment of the [AF]dG•del 11-mer duplex are listed for structure **1** in supplementary Table S4 and for structure **2** in supplementary Table S5. The following torsion angles deviate from standard B-DNA values for both conformations. The χ(O4′-C1′-N1-C2) glycosidic torsion of the dC5 residue is high *anti* rather than *anti* (structure **1**, $\chi = 310°$; structure **2**, $\chi = 313°$; normal *anti* $\chi \sim 240°$); the

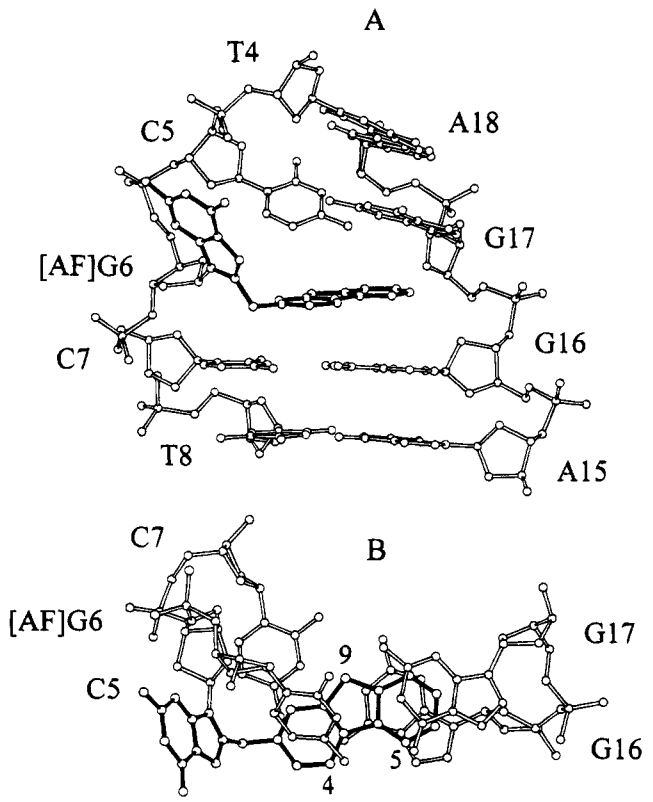

FIGURE 8: (A) Views looking into the major groove and normal to the helix axis of the central d(T4-C5-[AF]G6-C7-T8)·d(A15-G16-G17-A18) segment of structure **2** with the C^9-containing edge of AF directed toward the minor groove in the [AF]dG·del 11-mer duplex. The AF ring system is shown in darkened bonds and is intercalated between the dC5·dG17 and dC7·dG16 base pairs. The modified dG6 base is displaced into the major groove and is directed toward its 5′-neighbor dC5 in the sequence. (B) Views looking down the helix axis for the d(C5-[AF]G6-C7)·d(G16-G17) segment in the structure **2** of the [AF]dG·del 11-mer duplex. Figures were prepared using Molscript VI.1 (Kraulis, 1991).

ξ(O3′-P) torsion angle of the [AF]dG6 residue is between *gauche*$^+$ (60°) and *trans* (180°) rather than *gauche*$^-$ (300°) (structure **1**, $\xi = 136°$; structure **2**, $\xi = 134°$). The χ(O4′-C1′-N9-C4) glycosidic torsion angle of the [AF]dG6 residue is *syn* in both conformations, with values of $\chi = 64°$ in structure **1** and $\chi = 65°$ in structure **2**. The β(C5′-O5′) torsion of dC7 residue adopts values of $\beta = 112°$ in structure **1** and $\beta = 116°$ in structure **2**, respectively, in contrast to usual *trans* values in B-DNA. The pseudorotation parameter of the dG16 sugars are $\mathbf{P} = 53°$ in structure **1** and $\mathbf{P} = 63°$ in structure **2**, in the C4′-*exo* and C4′-*exo*/O1′-*endo* domain, respectively, in the [AF]dG·del 11-mer duplex. Other torsion angles and pseudorotation parameters for structures **1** and **2** are in or near ranges observed in B-DNA crystals (W. K. Olson, personal communication) (Table S4 and S5).

Convergence to very similar final structures for both structures **1** and **2** resulted when the NMR/energy-minimized structures were distorted by +45° or −45° at each of the two bonds (α′ and β′) at the base-carcinogen linkage and reminimized with restraints. Views of the best fit superposition of the resulting four structures for structure **1** are plotted in supplementary Figure S6 and for Structure **2** are plotted in supplementary Figure S7.

DISCUSSION

It has been possible to embark on structural studies for the [AF]dG6 adduct positioned opposite a deletion site in the d(C5-[AF]G6-C7)·d(G16-G17) sequence context due to the observation of narrow proton resonances for both the DNA and the aminofluorene ring in the [AF]dG·del 11-mer duplex. These proton resonances have been assigned and the carcinogen-DNA NOEs identified to provide sufficient restraints (Table 2) to define the solution structure at the [AF]dG·del site. The structural analysis was aided by the observed stabilization of the [AF]dG·del 11-mer duplex relative to its control dG·del 11-mer duplex enabling us to collect the experimental data at ambient temperature.

Syn Glycosidic Torsion Angle at Modified Guanine. The [AF]dG6 residue adopts a *syn* glycosidic alignment for interconverting structures **1** (Figure 7) and **2** (Figure 8) of the [AF]dG·del 11-mer duplex. The standard approach for distinguishing *syn* from *anti* guanine glycosidic torsion angles based on the magnitude of the NOE between the guanine H8 proton and its own sugar H1′ proton (Patel et al., 1982) cannot be used for [AF]dG6 since the H8 proton is replaced by the AF ring.

The [AF]dG6 glycosidic torsion angle was restricted to the *syn* range in the computations since the C1′ carbon of this modified guanine was shifted downfield by ~5 ppm from the corresponding chemical shifts of adjacent dG16 and dG17 guanine residues in the [AF]dG·del 11-mer duplex (Figure 5A). Such a large guanine C1′ downfield shift cannot originate from ring current contributions and instead has been identified with a *syn* glycosidic torsion angle for residues in the C2′-*endo* sugar pucker range (Greene et al., 1995).

The identification of a *syn* glycosidic torsion angle for [AF]dG6 is also supported by the unusual downfield chemical shift for the H2′ proton (3.34 ppm) of this modified residue in the [AF]dG·del 11-mer duplex (Figure 4). A similar downfield shift was detected for the H2′ proton of [AF]dG in the [AF]dG·dA 11-mer duplex studied previously for which an [AF]dG(*syn*)·dA(*anti*) alignment was established in solution (Norman et al., 1989).

Modified Guanine Displacement into the Major Groove. The modified guanine ring of [AF]dG6 is displaced into the major groove following intercalation of the AF ring into the helix opposite the −1 deletion site in structures **1** (Figure 7) and **2** (Figure 8) of the [AF]dG·del 11-mer duplex. The long axis of the displaced modified guanine is inclined relative to the helix axis such that one face stacks over the base and sugar major groove edges of the 5′-flanking dC5 while the other face is exposed to solvent. Such an alignment readily accounts for the experimentally observed upfield shifts of the major groove base (H6) and sugar (H2′ and H3′) protons of dC5 (Table S2) since these nonexchangeable protons are positioned over the modified guanine ring of [AF]dG6 and are shifted upfield due to ring current contributions.

The guanine imino proton of [AF]dG6 is exposed to solvent in the solution structures of the [AF]dG·del 11-mer duplex (Figures 7 and 8). This alignment readily explains the 11.26 ppm chemical shift for the imino proton of [AF]-dG6, which falls in a range characteristic of non-hydrogen-bonded imino protons. Further, the imino proton of [AF]dG6 exchanges rapidly with solvent water since we do not detect a diagonal cross-peak for this imino proton in the NOESY spectrum of the [AF]dG·del 11-mer duplex (Figure 2C), and instead a strong cross-peak is detected at the H_2O frequency (peak L, Figure 2B).

The two amino protons of [AF]dG6 are superpositioned at 6.31 ppm (Table 1), and a NOE is detected between the

imino and superpositioned amino protons for this modified residue (peak K, Figure 2B) in the [AF]dG·del 11-mer duplex. The averaged resonance for the amino protons of [AF]dG6 is consistent with both these exchangeable protons exposed to solvent rather than hydrogen-bonded to acceptor groups.

The sugar H1′, H2′, H2″, H3′, and H4′ protons of [AF]-dG6 are downfield relative to the same sugar protons for other residues in the d(C5-[AF]G6-C7)·d(G16-G17) segment of the [AF]dG·del 11-mer duplex (Table 1) consistent with displacement of the modified guanine out of the helix.

Intercalation of Aminofluorene Ring into the Helix. The aminofluorene ring intercalates into the helix between the dC5·dG17 and dC7·dG16 base pairs in structures **1** (Figure 7) and **2** (Figure 8) of the [AF]dG·del 11-mer duplex. Previous studies on [AF]dG aligned opposite dC in a DNA oligomer duplex have established that the aromatic AF protons resonate between 7.35 and 7.90 ppm when the AF ring is positioned outside the helix while the aromatic AF protons resonate between 6.65 and 7.60 ppm when the AF ring is intercalated between base pairs of the helix (Eckel & Krugh, 1994). The observed upfield shift of the AF protons in the intercalated-AF conformation must reflect ring current contributions from flanking base pairs that sandwich the intercalated AF ring. The aromatic AF protons resonate between 5.55 and 7.00 ppm in the [AF]dG·del 11-mer duplex (chemical shifts listed in the caption to Figure 3) consistent with intercalation of the AF ring into the helix. It is interesting that the aromatic AF protons for the [AF]dG·del alignment reported in this study are all further upfield [to the extent of 0.7−1.0 ppm for the AF(H1), AF(H6), AF-(H7), and AF(H8) protons] of their counterparts reported for the [AF]dG·dC alignment (Eckel & Krugh, 1994) even though the intercalated AF ring is stacked between adjacent base pairs in both alignments. These large shift differences must reflect the different orientation of the intercalated aminofluorene ring relative to the flanking base pairs when positioned opposite a deletion site (this study) as compared to positioning opposite a dC residue (Eckel & Krugh, 1994).

Intercalation of the AF ring into the DNA helix is established by the large number of carcinogen-DNA NOEs identified between the AF ring protons and the protons on the flanking dC5·dG17 and dC7·dG16 base pairs in the [AF]-dG·del 11-mer duplex (Table 2). The distribution of the carcinogen-DNA NOEs (Table 2) also establishes that the long axis of the aminofluorene ring is parallel to the long axis of the flanking dG·dC base pairs in structures **1** (Figure 7B) and **2** (Figure 8B) of the [AF]dG·del 11-mer duplex.

We do not detect NOEs between the imino protons of the dC5·dG17 and dC7·dG16 base pairs in the [AF]dG·del 11-mer duplex. This rules out a conformation where the AF ring and its attached modified guanine are both expelled out of the helix followed by collapse of the flanking dG·dC base pairs on each other.

Intercalation Site. The intercalation site is wedge-shaped with the dC5 and dC7 bases of the d(C5-[AF]G6-C7) segment on the modified strand separated by a greater distance than the dG16 and dG17 bases on the d(G16-G17) segment on the partner strand for both structures **1** (Figure 7A) and **2** (Figure 8A) of the [AF]dG·del 11-mer duplex.

The imino proton of dG17 (11.69 ppm) exhibits a greater line width in contrast to the imino protons of dG16 (11.98 ppm) in the proton spectrum of the [AF]dG·del 11-mer duplex at 1 and 15 °C (Figure S1). These data imply a selective perturbation of the Watson−Crick dC5·dG17 base pair at the intercalation site in the [AF]dG·del 11-mer duplex. Indeed, the Watson−Crick dC5·dG17 base pair exhibits both a large propeller twist and buckle in contrast to the Watson−Crick dC7·dG16 base pair that does not exhibit either propeller twist or buckle distortions in structures **1** (Figure 7A) and **2** (Figure 8A) of the [AF]dG·del 11-mer duplex.

We have identified chemical shift changes for protons and phosphorus resonances within the d(C5-[AF]G6-C7)·d(G16-G17) segment that forms the intercalation site in the [AF]-dG·del 11-mer duplex. The upfield shift of the imino protons of dG16 and dG17 to the 11.7−12.0 ppm range (Figure 1A) can be readily explained on the basis of their stacking over the aminofluorene ring in the AF-intercalated structures **1** (Figure 7B) and **2** (Figure 8B) of the [AF]dG·del 11-mer duplex. We have detected downfield shifted phosphorus resonances for the dC5-[AF]dG6 step on the modified strand and the dG16-dG17 step on the deletion containing strand at the intercalation site in the [AF]dG·del 11-mer duplex (Figure 5B).

Conformational Interconversion of AF Ring. Both the temperature dependence of the line shape of the proton spectra and the distribution of the carcinogen-DNA NOEs point toward a conformational interconversion of the AF ring between conformations designated **1** (Figure 7) and **2** (Figure 8). The nonexchangeable AF ring protons are narrow at 35 °C but broaden on lowering the temperature to 1 °C in the [AF]dG·del 11-mer duplex (Figure S3). These data are consistent with rapid interconversion between two conformations of the AF ring within the [AF]dG·del site at ambient temperature.

The distribution of carcinogen-DNA NOEs provides insights into these two interconverting conformations of the AF ring in the [AF]dG·del 11-mer duplex. Thus, both AF-(H1) positioned along one long edge of the AF ring and AF-(H3,H4) positioned along the opposite long edge of the AF ring exhibit NOEs to the [AF]dG6(H1′) and dC7(H1′) protons on the DNA (Table 2). This can only occur if the intercalated AF ring rapidly interconverts on the NMR time scale between alignments where its C^9-containing edge is positioned facing the major (structure **1**, Figure 7) and minor (structure **2**, Figure 8) grooves at the intercalation site. We cannot estimate the interconverting rate between the two conformations since we have been unable to slow the process sufficiently to monitor the NMR parameters of the individual conformations. A study of the structure of the [AF]dG·del 11-mer duplex by interactive computer graphics suggests a possible pathway for exchange between the two conformers, involving correlated rotational motions about the α' and β' torsion angles. A rotation about α' will move the aminofluorene out of the helix. This would then allow the approximately 180° rotation about β' to occur without steric clashes. Subsequent back-rotation around the α' torsion can then again place the aminofluorene ring within the helix. We have established that both dC5·dG17 and dC7·dG16 align through Watson−Crick pairing and that the former pair is distorted through propeller twisting and buckling in contrast to the latter unperturbed pair in the [AF]dG·del 11-mer duplex (Figures 7 and 8).

These results contrast with the demonstration of slow interconversion between intercalated-AF and external-AF conformations reported for the [AF]dG·dC alignment at the duplex level (Eckel & Krugh, 1994). This is not surprising since a higher barrier is expected in this case where both

the AF ring and the attached dG base are involved in the conformational interconversion, which in one case inserts the AF ring and in the other inserts the dG ring into the helix.

Comparison of Intercalated-AF Conformations. A recent NMR-based structural study defined an equilibrium between external-AF and intercalated-AF conformations in slow exchange for the case of [AF]dG positioned opposite dC in the sequence context d(A-[AF]G-G)·d(C-C-T) at the duplex level (Eckel & Krugh, 1994). Based on the assumption of an *anti* glycosidic torsion angle at the [AF]dG residue, these authors concluded that intercalation of the AF residue resulted in base displacement of the modified guanine into the minor groove in the intercalated-AF conformation.

It should be noted that this conclusion of base displacement of the modified guanine in an *anti* alignment into the minor groove for the intercalated-AF conformation in the case of [AF]dG positioned opposite dC (Eckel & Krugh, 1994) contrasts with our demonstration of base displacement of the modified guanine in a *syn* alignment into the major groove for the intercalated-AF conformation in the case of [AF]dG positioned opposite a deletion site (this study). We are confident in our application of sugar ^{13}C chemical shifts to distinguish between *syn* and *anti* alignments of [AF]dG positioned opposite a deletion site reported in this study.

Comparison of [AF]-C^8-dG and [BP]-N^2-dG Adducts Positioned Opposite Deletion Sites. We have recently reported on the solution structures of (+)-*trans-anti*-[BP]-N^2-dG and (+)-*cis-anti*-[BP]-N^2-dG adducts positioned opposite deletion sites in the d(C5-[BP]G6-C7)·d(G16-G17) sequence context (Cosman et al., 1994a,b), which is identical to that used in the current study of the [AF]-C^8-dG adduct positioned opposite a deletion site. The key difference between these two adducts is that the benzo[*a*]pyrenyl ring is covalently linked through the N^2-exocyclic amino group of guanine while the aminofluorene ring is covalently linked through the C^8-position of guanine.

Despite these pronounced differences in the covalent linkage site position, there are similarities in the structural motifs determined for the (+)-*trans-anti*-[BP]-N^2-dG·del (Figure 9B) (Cosman et al., 1994a) and [AF]-C^8-dG·del (Figure 9A) (this study) at the oligomer duplex level. In both cases, the aromatic chromophores intercalate into the helix between flanking dG·dC pairs opposite the deletion site, and this is accompanied by displacement of the modified guanine into the major groove. The important difference between the alignment of the two adducts is the *syn* glycosidic torsion angle at the [AF]-C^8-dG·del site (Figure 9A) in contrast to the *anti* glycosidic torsion angle at the (+)-*trans-anti*-[BP]-N^2-dG·del site (Figure 9B) in the same sequence context. In addition, the long axis of the intercalated AF ring is parallel to that of the flanking dG·dC base pairs (Figure 9A), in contrast to the orthogonal alignment of the long axis of the intercalated BP ring and flanking dG·dC base pairs (Figure 9B).

These results emphasize that the hydrophobic aromatic rings of both the polycyclic aromatic hydrocarbon and the heterocyclic aromatic amine when covalently linked to guanines preferentially intercalate into the helix opposite −1 deletion sites and stack with flanking base pairs. The modified guanine ring is displaced into the major groove and stacks over the 5′-side cytosine base in either *anti* or *syn* glycosidic torsion angle alignments depending on whether the covalent linkage site of the adducts is N^2 or C^8, respectively.

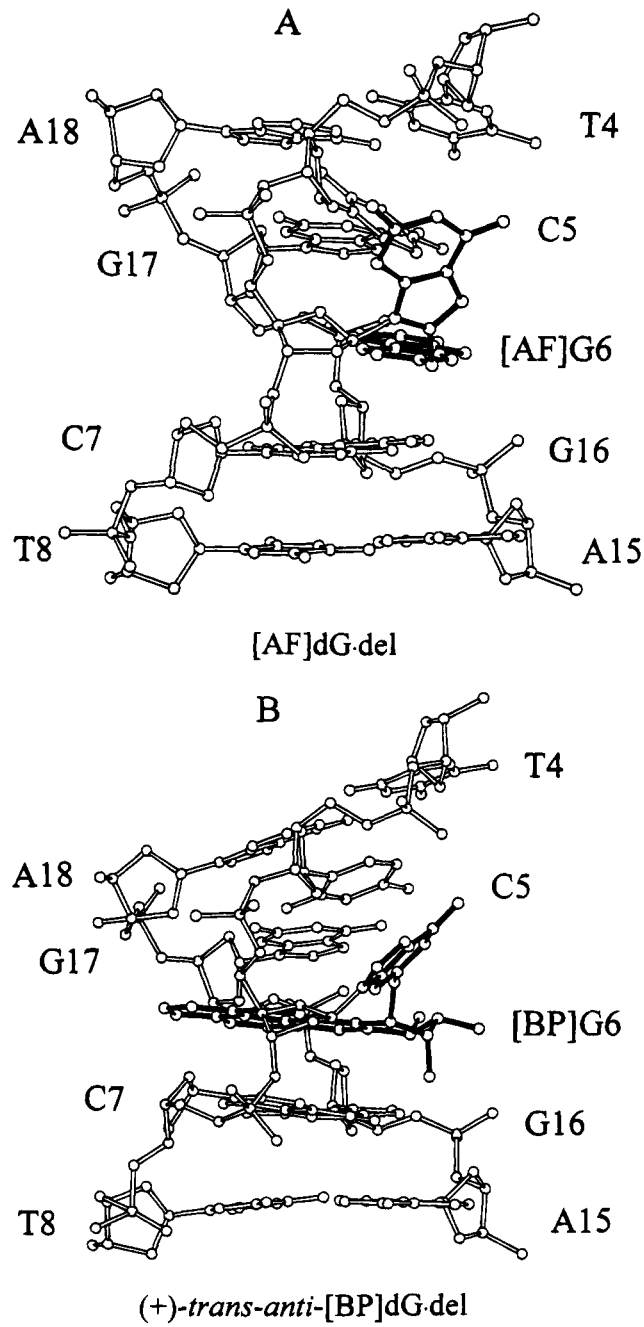

FIGURE 9: Comparative views of the solution structures of (A) the d(T4-C5-[AF]G6-C7-T8)·d(A15-G16-G17-A18) segment of the [AF]dG·del 11-mer duplex (structure **1**, this study) and (B) the d(T4-C5-[BP]G6-C7-T8)·d(A15-G16-G17-A18) segment of the (+)-*trans-anti*-[BP]dG·del 11-mer duplex (Cosman et al., 1994a). The [AF]dG6 and [BP]dG6 residues are shown in darkened bonds. Figures were prepared using Molscript VI.1 (Kraulis, 1991).

Biological Significance. A slippage mechanism to explain −1 deletions during replication of carcinogen−DNA adducts has been proposed in recent years (Kunkel, 1990; Schaaper et al., 1990; Shibutani & Grollman, 1993; Napolitano et al., 1994) based on the original suggestion of Streisinger et al. (1966) for unmodified DNA. The details of the mechanism depend on the specific sequence context of the lesion.

Applied to the present d(C-[AF]G-C) sequence, replication proceeds to the lesion site, and a dG is inserted opposite the damaged template guanine. Replication stalls at this point,

as the adduct hinders insertion of the next nucleotide. The delay in replication provides time for a rearrangement in which the carcinogen-bound guanine bulges out of the helix, and the mismatched partner guanine on the primer strand pairs with the 5′ cytosine of the template. Replication then continues normally to afford a duplex with an adducted base that is unpartnered; this is an extended bulge structure in which the newly synthesized strand has suffered a deletion. Repair enzymes could correct the bulge-out, but if this failed, the deletion would be permanent after another round of replication.

Thermodynamic studies on carcinogen-adducted duplexes of this extended bulge type reveal stabilization of the modified duplex compared to the unmodified one (Garcia et al., 1993; Ya et al., 1994), which lends support to this proposed type of mechanism for −1 deletions.

The present study affords a high-resolution view of the extended bulge in an aromatic amine adduct to C^8 of guanine. Interestingly, it shares important structural features with the (+)-*trans-anti-* and (+)-*cis-anti*-benzo[*a*]pyrene diol epoxide adducts to guanine N^2 in −1 deletion duplexes (Cosman et al., 1994a,b) in adopting a base-displacement intercalation-type conformation. This suggests the possibility of a common structural origin on the three-dimensional level for −1 deletions in polycyclic aromatic carcinogens, which could be independent of the linkage site.

ACKNOWLEDGMENT

We thank Wilma K. Olson for sharing her unpublished analysis of pseudorotation parameters in nucleic acid crystal structures.

SUPPLEMENTARY MATERIAL AVAILABLE

Five tables listing exchangeable and nonexchangeable proton chemical shifts for the entire [AF]dG·del 11-mer adduct duplex, proton chemical shift differences on adduct formation, and backbone torsion angles for the central segment of the energy minimized structures of both conformers of the [AF]dG·del 11-mer duplex and seven figures showing the temperature dependent exchangeable and nonexchangeable proton spectra for the [AF]dG·del 11-mer duplex, the unrestrained structures of the entire adduct duplexes, and the superposition of four structures derived following energy minimization with restraints from the two restrained structures **1** and **2** in which the α′ and β′ angles were changed by ±45° (15 pages). Ordering information is given on any current masthead page.

REFERENCES

Altona, C., & Sundaralingam, M. (1972) *J. Am. Chem. Soc. 94*, 8205−8212.
Arnott, S., Bond, P. J., Selsing, E., & Smith, P. J. (1976) *Nucleic Acids Res. 2*, 2459−2470.
Babcock, M. S., Pednault, E. P. D., & Olson, W. K. (1993) *J. Biomol. Struct. Dyn. 11*, 597−628.
Bax, A., & Subramanian, J. (1986) *J. Magn. Reson. 67*, 565−570.
Belguise-Valladier, P., & Fuchs, R. P. P. (1991) *Biochemistry 30*, 10091−10100.
Belguise-Valladier, P., Maki, H., Sekiguchi, M., & Fuchs, R. P. P. (1994) *J. Mol. Biol. 236*, 151−164.
Bichara, M., & Fuchs, R. P. P. (1985) *J. Mol. Biol. 183*, 341−351.
Broyde, S., & Hingerty, B. E. (1983) *Biopolymers 22*, 2423−2441.
Burnouf, D., Koehl, P., & Fuchs, R. P. P. (1989) *Proc. Natl. Acad. Sci. U.S.A. 86*, 4147−4151.
Carothers, A. M., Steigerwalt, R. W., Urlaub, G., Chasin, L. A., & Grunberger, D. (1989) *J. Mol. Biol. 208*, 417−428.
Cho, B. P., Beland, F. A., & Marques, M. M. (1994) *Biochemistry 33*, 1373−1384.
Cosman, M., de los Santos, C., Fiala, R., Hingerty, B. E., Ibanez, V., Luna, E., Harvey, R., Geacintov, N. E., Broyde, S., & Patel, D. J. (1993) *Biochemistry 32*, 4145−4155.
Cosman, M., Fiala, R., Hingerty, B. E., Amin, S., Geacintov, N. E., Broyde, S., & Patel, D. J. (1994a) *Biochemistry 33*, 11507−11517.
Cosman, M., Fiala, R., Hingerty, B. E., Amin, S., Geacintov, N. E., Broyde, S., & Patel, D. J. (1994b) *Biochemistry 33*, 11518−11527.
Eckel, L. M., & Krugh, T. R. (1994) *Biochemistry 33*, 13611−13624.
Garcia, A., Lambert, I. B., & Fuchs, R. P. P. (1993) *Proc. Natl. Acad. Sci. U.S.A. 90*, 5989−5993.
Ghose, R., Marino, J. P., Wiberg, K. B., & Prestegard, J. H. (1994) *J. Am. Chem. Soc. 116*, 8827−8828.
Greene, K. L., Wang, Y., & Live, D. (1995) *J. Biomol. NMR* (in press).
Gupta, P. K., Johnson, D. L., Reid, T. M., Lee, M.-S., Romano, L. J., & King, C. M. (1989) *J. Biol. Chem. 264*, 20120−20130.
Gupta, P. K., Pandrangi, R. G., Lee, M.-S., & King, C. M. (1991) *Carcinogenesis 12*, 819−824.
Heflich, R. H., & Neft, R. E. (1994) *Mutat. Res. 318*, 73−174.
Hingerty, B. E., & Broyde, S. (1982) *Biochemistry 21*, 3243−3252.
Hingerty, B. E., Figueroa, S., Hayden, T., & Broyde, S. (1989) *Biopolymers 28*, 1195−1222.
Kraulis, P. J. (1991) *J. Appl. Crystallogr. 24*, 946−950.
Kunkel, T. A. (1990) *Biochemistry 29*, 8003−8011.
Lambert, I. B., Napolitano, R. L., & Fuchs, R. P. P. (1992) *Proc. Natl. Acad. Sci. U.S.A. 89*, 1310−1314.
Mah, M. C.-M., Boldt, J., Culp, S. J., Maher, V. M., & McCormick, J. J. (1991) *Proc. Natl. Acad. Sci. U.S.A. 88*, 10193−10197.
Melchior, W. B., Jr., Marques, M. M., & Beland, F. A. (1994) *Carcinogenesis 15*, 889−899.
Moriya, M., Takeshita, M., Johnson, F., Peden, K., Will, S., & Grollman, A. P. (1988) *Proc. Natl. Acad. Sci. U.S.A. 85*, 1586−1589.
Napolitano, R. L., Lambert, I. B., & Fuchs, R. P. P. (1994) *Biochemistry 33*, 1311−1315.
Norman, D., Abuaf, P., Hingerty, B. E., Live, D., Grunberger, D., Broyde, S., & Patel, D. J. (1989) *Biochemistry 28*, 7462−7476.
Patel, D. J., Kozlowski, S. A., Nordheim, A., & Rich, A. (1982) *Proc. Natl. Acad. Sci. U.S.A. 79*, 1413−1417.
Schaaper, R. M., Koffel-Schwartz, N., & Fuchs, R. P. (1990) *Carcinogenesis, 11*, 1087−1095.
Schlick, T., Hingerty, B. E., Peskin, C. S., Overton, M. L., & Broyde, S. (1990) in *Theoretical Chemistry and Molecular Biophysics* (Beveridge, D., & Lavery, R., Eds.) pp 39−58, Academic Press, New York.
Shibutani, S., & Grollman, A. P. (1993) *J. Biol. Chem. 268*, 11703−11710.
Singh, S. B., Hingerty, B. E., Singh, U. C., Greenberg, J. P., Geacintov, N. E., & Broyde, S. (1991) *Cancer Res. 51*, 3482−3492.
Sklenar, V., Miyashiro, H., Zon, G., Miles, H. T., & Bax, A. (1986) *FEBS Lett. 208*, 94−98.
Streisinger, G., Okada, Y., Emrich, J., Newton, J., Tsugita, A., Terzaghi, E., & Inouye, M. (1966) *Cold Spring Harbor Symp. Quant. Biol. 31*, 77−84.
Taylor, E. R., & Olson, W. K. (1983) *Biopolymers 22*, 2667−2702.
Tebbs, R.-S., & Romano, L. J. (1994) *Biochemistry 33*, 8998−9006.
Thomas, D. C., Veaute, X., Kunkel, T. A., & Fuchs, R. P. P. (1994) *Proc. Natl. Acad. Sci. U.S.A. 91*, 7752−7756.
van de Ven, F. J., & Hilbers, C. W. (1988) *Eur. J. Biochem. 178*, 1−38.
Varani, G., & Tinoco, I. Jr. (1991) *J. Am. Chem. Soc. 113*, 9349−9354.
Ya, N.-Q., Smirnov, S., Cosman, M., Bhanot, S., Ibanez, V., & Geacintov, N. E. (1994) *Structural Biology: The State of the Art* (Sarma, R.-H., & Sarma, M., Eds.) Vol. 2, pp 349−366, Adenine Press, Schenectady, NY.

BI950014V